Astron. Astrophys. 363, 1055–1064 (2000)

ASTRONOMY AND ASTROPHYSICS

X-ray irradiated model stellar atmospheres

II. Comprehensive treatment of Compton scattering

J. Madej[1] **and A. Różańska**[2]

[1] Astronomical Observatory, University of Warsaw, Al. Ujazdowskie 4, PL-00-478 Warsaw, Poland (jm@cirrus.astrouw.edu.pl)
[2] Copernicus Astronomical Center, Bartycka 18, PL-00-716 Warsaw, Poland (agata@camk.edu.pl)

Received 15 June 2000 / Accepted 4 October 2000

Abstract. We present equations and details of the computer code for model atmosphere computations, in which we include both nonzero external illumination by very hard X-rays, and Compton scattering opacity and emissivity. We assume both radiative and hydrostatic equilibrium, and LTE equation of state. The code solves simultaneously transfer of thermal radiation emitted by a hot main sequence stellar atmosphere and incident hard X-rays of photon energy approaching electron rest mass.

The equation of radiative transfer and remaining equations of equilibrium contain Compton scattering terms appropriate for scattering of photons of arbitrarily large initial energies. In our paper we consider Compton scattering of photons of energy up to 400 keV on free electrons in fully relativistic thermal motion.

In this paper we consider illumination of a B3 V type star by isotropic X-rays of diluted thermal spectral distribution with temperature $T_{rad} = 10^8$ K. Two series of models are computed, hydrogen-helium models and iron rich models. Our results demonstrate, that the external illumination causes extreme temperature rise at least in the uppermost layers. Outgoing spectra exhibit: big UV bump, numerous H, He, and Fe b-f opacity jumps mostly in emission, and also reflected incident spectrum with Compton cut-off. The model spectra also reflect qualitatively spectral properties of the active galactic nuclei (AGN).

Key words: radiative transfer – scattering – stars: atmospheres – galaxies: active

1. Introduction

Effects of Compton scattering of X-rays on free electrons are very important in stellar atmospheres at various effective temperatures. In bursting neutron stars ($T_{eff} \sim 10^7$ K), or even in the hottest white dwarf stars ($T_{eff} \sim 10^5$ K), X-rays are created by thermal processes in the atmosphere. In case of cooler atmospheres, one can consider scattering of X-rays incoming from some external source. The latter is the subject of our paper, in which we formulate equations of model atmosphere and radiative transfer.

Send offprint requests to: A. Różańska

Our approach to the Compton scattering is valid for photons of arbitrarily large initial energies, which are subsequently scattered by electrons in fully relativistic thermal motion (Pomraning 1973). The equations are also suitable to the situation, when Compton scattering dominates other opacity sources. In each iteration step our code computes coefficient of scattering opacity from relativistic formulae, thus avoiding Klein-Nishina expression, the latter valid only for the scattering from electrons at rest. The equations were formulated and described in detail by Madej (1991, hereafter Paper I). However, algebraic decomposition of integro-differential equations and elimination scheme used here are taken after Madej & Różańska (2000), hereafter Paper II, and are significantly changed as compared with Paper I. In the following sections most of equations are just reminded, while we do not present their detailed derivation.

In this paper we consider the structure and the spectrum of a hot main sequence B star ($T_{eff} = 1.8 \times 10^4$ K and $\log g = 4.0$, cgs units), illuminated from outside by very hot diluted thermal X-rays ($T_{rad} = 10^8$ K). Two series of models were computed, the first one consisting of hydrogen and helium in solar proportions, and the second one including also iron with number abundance $N_{Fe}/N_H = 3.7 \times 10^{-5}$. Transfer of radiation is solved with the method of variable Eddington factors. External illumination was included in the equation of transfer following the method by Ruciński (1970). All the models assume LTE equation of state.

This paper is a substantial extension of our previous research (Paper II), in which we have presented and solved set of equations defining a model atmosphere in radiative and hydrostatic equilibrium, exposed to the external radiation field. In Paper II we assumed that electron scattering is fully coherent (Thomson scattering). This restrictive assumption did not allow for realistic reproduction of the external illumination effects. In the present paper we append Compton scattering terms to the model atmosphere equations, leaving method of solution essentially unchanged.

Our code is a general purpose computer program and can be used for a wide variety of problems. Optionally, Compton scattering can be replaced by Thomson scattering without changing model equations. Also the external illumination can be simply set to zero for model atmosphere computations of single stars.

The code can be used for the study of illumination effects in close binary stars, and the atmospheres of accretion disks in active galactic nuclei (AGN), and cataclysmic variables (CV). However, in case of an accretion disk the energy dissipation via viscosity should be taken into account (cf. Hubeny 1990a). We plan to study this problem in future work.

2. Compton scattering in AGN

It is widely believed that the production of soft X-ray excess in AGN (Active Galactic Nuclei), and hard X-ray tail in both AGN and GBHs (Galactic Black Holes) continuum spectra are caused by Comptonization.

The observed hard X-ray spectra of those objects consist of primary power-law X-ray radiation emitted from the hot plasma, and Compton reflection bump (for a review see Mushotzky et al. 1993 for AGN, and Tanaka & Lewin 1995 for GBHs). The former component results from Compton cooling of hot, probably thermal plasma by soft photons incoming from the accretion disk. Compton reflection bump exhibits K_α line with energy about 6.4 keV, which implies that the reflecting matter is cold, $\sim 10^5$ K. High energy cut-off is observed at ~ 100 keV. The latter feature results from two physical reasons. First of all, for high energy photons the cross-section decreases with increasing photon energy, therefore probability of interaction with electrons decreases. However, if scattering occurred, then photon loses all its energy at the time of Compton scattering on cold electrons (Rybicki & Lightman 1979).

Approximately 10 per cent of hard X-ray photons is reflected, while the remaining 90 per cent is absorbed by cold matter, and energy of these photons is reemitted in soft X-ray band. This is the most probable explanation of soft X-ray excess, which appears as significant low energy ($\lesssim 1$ keV) spectral steepening. Such a feature is widely observed in radio-quiet AGN (Turner & Pounds 1989; Walter & Fink 1993).

Therefore, it is very important to calculate spectra from illuminated disk atmospheres with account of Compton scattering. Many attempts were done on this subject, however, the problem is extremely complex. It is very difficult to compute the structure and spectra of optically thick media self-consistently, taking into account both process of Comptonization and absorption of hard X-ray radiation.

In the existing codes calculating spectrum of the illuminated disk atmosphere, Compton scattering was treated in three different ways. The scattering could be roughly approximated by the local heating and cooling rates, as was done in the photoionization codes CLOUDY, XSTAR and MAPPING. The above approach could be easily implemented also in few radiative transfer calculations (Ko & Kallman 1994; Collin-Souffrin et al. 1996; Sincell & Krolik 1997).

In other approach one solved the Kompaneets equation as part of the radiative transport equation, but it was usually done only for fully ionized hydrogen and helium disk, i.e. neglecting absorption (Shimura et al. 1995). In other papers their authors added some absorption, but only in uniform slab of matter (Ross & Fabian 1993; Matt et al. 1993). Most recently Nayakshin et al. (2000) used modified Kompaneets equation with approximate Compton scattering redistribution function for the computations of disk structure in hydrostatic equilibrium. Nevertheless, Kompaneets equation can approximate only Compton scattering on electrons in non-relativistic thermal motion.

Up to now, the most advanced approach to the Comptonization in illuminated accretion disk was done by Życki et al. (1994), who presented Monte Carlo simulations. However, their computations treated slab of matter with constant density.

Our approach to Compton scattering is much more general, since it is suitable for photons and electrons of any energies and allows to calculate the structure of an atmosphere both in hydrostatic and radiative equilibrium. I.e. in models presented below we apply the full art of model stellar atmosphere computations. Our code can be easily used for the accretion disk atmospheres, assuming that all the energy has been generated below the thermalization depth via viscosity. We are able to compute self consistently the structure and outgoing spectra, to precisely reproduce reflection and redistribution of external X-rays towards longer wavelengths. We include here hydrogen, helium and iron, all these elements considered in every possible ionization state.

3. The equation of transfer

The key element and starting point in our research is a realistic expression for the differential Compton scattering cross section $\sigma(\nu \to \nu', \mathbf{n}\cdot\mathbf{n}')$, describing scattering by electrons in relativistic thermal motion. In this research we adopted formulae from Guilbert (1981). The differential cross section can be decomposed according to

$$\sigma(\nu \to \nu', \mathbf{n}\cdot\mathbf{n}') = \sigma_\nu \, \phi\,(\nu, \nu', \mathbf{n}\cdot\mathbf{n}')\,, \tag{1}$$

where variable σ_ν denotes the total Compton scattering cross section (in cm^2). Variable ϕ denotes the scattering redistribution function (scattering kernel), normalized to unity

$$\int\limits_0^\infty d\nu' \oint\limits_{\omega'} \phi\,(\nu, \nu', \mathbf{n}\cdot\mathbf{n}')\,\frac{d\omega'}{4\pi} = \int\limits_0^\infty \Phi(\nu, \nu')\,d\nu' = 1\,. \tag{2}$$

In the following equations we shall use the function Φ, which is defined as the zeroth angular moment of ϕ (Pomraning 1973).

We introduce auxiliary functions Φ_1 and Φ_2, which are defined by

$$\Phi_1(\nu, \nu') = \left[1 + \frac{c^2}{2h\nu'^3}(J_{\nu'} + U_{\nu'})\right]\,\Phi(\nu, \nu')\,, \tag{3}$$

$$\begin{aligned}\Phi_2(\nu, \nu') \;&=\; \left[1 + \frac{c^2}{2h\nu^3}(J_\nu + U_\nu)\right]\,\left(\frac{\nu}{\nu'}\right)^3 \times \\ &\quad \times \exp\left[-\frac{h(\nu-\nu')}{kT}\right]\,\Phi(\nu, \nu') \\ &=\; \left[1 + \frac{c^2}{2h\nu^3}(J_\nu + U_\nu)\right]\,\frac{\nu}{\nu'}\,\Phi(\nu', \nu)\,.\end{aligned} \tag{4}$$

Both functions Φ_1 and Φ_2 contain stimulated scattering correction factors, and fulfil strictly the detailed balancing condition in thermodynamic equilibrium (cf. Paper I).

We assume the following time-independent equation of radiative transfer, suitable for planar geometry

$$\mu \frac{\partial I_\nu}{\partial \tau_\nu} = I_\nu - \epsilon_\nu B_\nu - (1-\epsilon_\nu) J_\nu + \\ + (1-\epsilon_\nu) J_\nu \int_0^\infty \Phi_1(\nu,\nu')\, d\nu' - \\ - (1-\epsilon_\nu) \int_0^\infty (J_{\nu'} + U_{\nu'})\, \Phi_2(\nu,\nu')\, d\nu' , \quad (5)$$

where we included both thermal and scattering emission. We assume here nongrey true absorption κ_ν, and noncoherent Compton scattering opacity, σ_ν, both taken for 1 gram. Absorption coefficient κ_ν included already LTE stimulated emission. Dimensionless absorption $\epsilon_\nu = \kappa_\nu/(\kappa_\nu + \sigma_\nu)$.

Variable U_ν denotes the mean intensity of external irradiation at the level τ_ν, with $d\omega = d\mu_\omega d\phi_\omega$

$$U_\nu(\tau_\nu) = \frac{1}{4\pi} \int_\Omega I_\nu^{ext}(\omega)\, \exp(-\tau_\nu/\mu_\omega)\, d\omega , \quad (6)$$

and variable V_ν denotes the flux

$$V_\nu(\tau_\nu) = \frac{1}{4\pi} \int_\Omega I_\nu^{ext}(\omega)\, \mu_\omega\, \exp(-\tau_\nu/\mu_\omega)\, d\omega . \quad (7)$$

Following the standard approach we compute zeroth and first momenta of the equation of transfer

$$\frac{dH_\nu}{d\tau_\nu} = \epsilon_\nu (J_\nu - B_\nu) + (1-\epsilon_\nu) J_\nu \int_0^\infty \Phi_1(\nu,\nu')\, d\nu' - \\ - (1-\epsilon_\nu) \int_0^\infty (J_{\nu'} + U_{\nu'})\, \Phi_2(\nu,\nu')\, d\nu' , \quad (8)$$

$$\frac{dK_\nu}{d\tau_\nu} = H_\nu . \quad (9)$$

3.1. Radiative equilibrium

The constraint of radiative equilibrium implies on each depth level τ_ν that

$$\int_0^\infty H_\nu(\tau_\nu)\, d\nu - \int_0^\infty V_\nu(\tau_\nu)\, d\nu = \frac{\sigma_R T_{eff}^4}{4\pi} , \quad (10)$$

where $\sigma_R = 5.66961 \times 10^{-5}$ (cgs units). Taking derivative $d/d\tau = d/d\tau_\nu\ (d\tau_\nu/d\tau)$ of the above equation, we obtain the alternative form of the equation of radiative equilibrium

$$\int_0^\infty \eta_\nu \epsilon_\nu (J_\nu + U_\nu - B_\nu^*)\, d\nu + \\ + \int_0^\infty \eta_\nu (1-\epsilon_\nu)(J_\nu + U_\nu)\, d\nu \int_0^\infty \Phi_1^*(\nu,\nu')\, d\nu' \\ - \int_0^\infty \eta_\nu (1-\epsilon_\nu)\, d\nu \int_0^\infty (J_{\nu'} + U_{\nu'})\, \Phi_2^*(\nu,\nu')\, d\nu' = 0 ,$$

where $\eta_\nu = (\kappa_\nu + \sigma_\nu)/(\kappa+\sigma)_{std}$. Functions B_ν^*, Φ_1^*, and Φ_2^* are computed at the unknown temperature T^*, in which they fulfil strictly the constraint of radiative equilibrium.

3.2. Hydrostatic equilibrium

The total scalar pressure $P = P_g + P_r$, and the gradient of gas pressure in hydrostatic equilibrium is given by

$$\frac{dP_g}{d\tau} = \frac{g}{(\kappa+\sigma)_{std}} - \frac{dP_r}{d\tau} = \\ = \frac{g}{(\kappa+\sigma)_{std}} - \frac{4\pi}{c} \int_0^\infty \eta_\nu\, (H_\nu - V_\nu)\, d\nu , \quad (12)$$

see also Paper II for more details.

3.3. Temperature corrections

We assume linear Taylor expansions

$$B_\nu^*(\tau) = B_\nu(\tau) + \left(\frac{\partial B_\nu}{\partial T}\right)_\tau \Delta T(\tau) , \quad (13)$$

$$\Phi_1^*(\nu,\nu') = \Phi_1(\nu,\nu') + \left(\frac{\partial \Phi_1}{\partial T}\right)_\tau \Delta T(\tau) , \quad (14)$$

$$\Phi_2^*(\nu,\nu') = \Phi_2(\nu,\nu') + \left(\frac{\partial \Phi_2}{\partial T}\right)_\tau \Delta T(\tau) , \quad (15)$$

where $\Delta T = T^* - T$, variables T and T^* denoting the actual and final values of temperature, respectively. We follow here the standard strategy of model stellar atmosphere computations, where changes of various physical variables are represented by linear perturbations, and nonlinear (quadratic) terms are neglected. This method was proven by many numerical experiments to be efficient, general, and stable (Mihalas 1978, p. 180).

Then, we immediately obtain linear temperature corrections

$$\Delta T(\tau) = \frac{\int_0^\infty \eta_\nu \epsilon_\nu\, (J_\nu + U_\nu - B_\nu)\, d\nu + L(\tau)}{\int_0^\infty \eta_\nu \epsilon_\nu\, (\partial B_\nu/\partial T)_\tau\, d\nu - L'(\tau)} . \quad (16)$$

The sum $J_\nu + U_\nu$ equals the total mean intensity of radiation on the level τ_ν. New functions, $L(\tau)$ and $L'(\tau)$, are defined by

$$L(\tau) = \int_0^\infty \eta_\nu (1-\epsilon_\nu)(J_\nu + U_\nu)\, d\nu \int_0^\infty \Phi_1(\nu,\nu')\, d\nu' \\ - \int_0^\infty \eta_\nu (1-\epsilon_\nu)\, d\nu \int_0^\infty (J_{\nu'} + U_{\nu'}) \Phi_2(\nu,\nu')\, d\nu' , \quad (17)$$

$$L'(\tau) = \int_0^\infty \eta_\nu(1-\epsilon_\nu)(J_\nu+U_\nu)\,d\nu \int_0^\infty \Phi_1'(\nu,\nu')\,d\nu' \quad (18)$$
$$- \int_0^\infty \eta_\nu(1-\epsilon_\nu)\,d\nu \int_0^\infty (J_{\nu'}+U_{\nu'})\Phi_2'(\nu,\nu')\,d\nu' .$$

Variables Φ_i', $i=1$ or 2, denote partial derivatives of the redistribution functions with respect to temperature

$$\Phi_1'(\nu,\nu') = \left[1+\frac{c^2}{2h\nu'^3}(J_{\nu'}+U_{\nu'})\right]\left(\frac{\partial\Phi}{\partial T}\right)_\tau , \quad (19)$$

and

$$\Phi_2'(\nu,\nu') = \left[1+\frac{c^2}{2h\nu^3}(J_\nu+U_\nu)\right]\left(\frac{\nu}{\nu'}\right)^3 \times$$
$$\times \left[\left(\frac{\partial\Phi}{\partial T}\right)_\tau + \frac{h\Delta\nu}{kT^2}\,\Phi(\nu,\nu')\right]\exp\left(-\frac{h\Delta\nu}{kT}\right)$$
$$= \left[1+\frac{c^2}{2h\nu^3}(J_\nu+U_\nu)\right]\frac{\nu}{\nu'}\,\Phi'(\nu',\nu) , \quad (20)$$

where $\Delta\nu=\nu-\nu'$. In thermodynamic equilibrium ($J_\nu=B_\nu$, and $U_\nu=0$) we must have $L=0$.

3.4. The equation of transfer and boundary conditions

Following the standard procedure we combine Eqs. 8 – 9 and get

$$\frac{d^2}{d\tau_\nu^2}(f_\nu J_\nu) = \epsilon_\nu(J_\nu-B_\nu^*) + (1-\epsilon_\nu)J_\nu\int_0^\infty \Phi_1^*(\nu,\nu')\,d\nu'$$
$$- (1-\epsilon_\nu)\int_0^\infty (J_{\nu'}+U_{\nu'})\,\Phi_2^*(\nu,\nu')\,d\nu' . \quad (21)$$

Such an equation implicitly contains unknown temperature corrections ΔT. Eddington factors $f_\nu = K_\nu/J_\nu$. The final form of the equation of transfer is

$$\frac{d^2}{d\tau_\nu^2}(f_\nu J_\nu) = \epsilon_\nu(J_\nu-B_\nu) + (1-\epsilon_\nu)J_\nu\int_0^\infty \Phi_1(\nu,\nu')\,d\nu'$$
$$- (1-\epsilon_\nu)\int_0^\infty (J_{\nu'}+U_{\nu'})\,\Phi_2(\nu,\nu')\,d\nu'$$
$$- \left[\epsilon_\nu\frac{\partial B_\nu}{\partial T} - (1-\epsilon_\nu)(J_\nu+U_\nu)\int_0^\infty \frac{\partial\Phi_1}{\partial T}\,d\nu'\right.$$
$$\left. + (1-\epsilon_\nu)\int_0^\infty (J_{\nu'}+U_{\nu'})\frac{\partial\Phi_2}{\partial T}\,d\nu'\right]\times$$
$$\times \frac{\int_0^\infty \eta_\nu\epsilon_\nu(J_\nu+U_\nu-B_\nu)\,d\nu + L(\tau)}{\int_0^\infty \eta_\nu\epsilon_\nu(\partial B_\nu/\partial T)_\tau\,d\nu - L'(\tau)} . \quad (22)$$

The above linearized equation of transfer was solved in the actual model stellar atmosphere computations.

a. At the upper boundary we apply the equation which directly results from the equation for momenta, Eq. 9

$$\frac{\partial}{\partial\tau_\nu}(f_\nu J_\nu) = h_\nu J_\nu(0) . \quad (23)$$

The surface factor $h_\nu = H_\nu(0)/J_\nu(0)$, which is equal to $h_\nu = 0.5$ in the initial Eddington approximation. The above upper boundary condition is just a relation between the surface mean intensity and the flux. Factors h_ν can be iterated to exact, frequency-dependent values simultaneously with variable Eddington factors f_ν (Mihalas 1978).

Note, that the upper boundary condition, Eq. 23, is formally the same as for a nonilluminated atmosphere. This is because the external illumination was explicitly separated in the equation of transfer, Eq. 6.

b. At the lower boundary we assume the diffusion approximation

$$\frac{\partial}{\partial\tau_\nu}(f_\nu J_\nu) = \frac{1}{3}\frac{\partial B_\nu}{\partial\tau_\nu} . \quad (24)$$

Useful form of that condition and its derivation is given in the Appendix.

3.5. Computational details

Full set of model atmosphere equations solved in this paper consists of discretized radiative transfer Eqs. (22), written on frequencies $\nu_i, i=1,\ldots,I$, supplemented by the equation of hydrostatic equilibrium (12), and the equation for new temperatures $T = T^* + \Delta T$, with ΔT given by Eq. (16). The LTE equation of state for ideal gas, and expressions for monochromatic opacities close the whole system.

Actual model computations were performed with the two numerical assumptions:

– For simplicity, electron scattering cross section per one particle has been set to Thomson value, 6.65×10^{-25} cm^2. However, the normalized redistribution functions ϕ were always precisely reconstructed for each discrete frequency and temperature.

– To avoid convergence problems, two Compton scattering terms in the equation of transfer,

$$(J_\nu+U_\nu)\int_0^\infty \Phi_1(\nu,\nu')\,d\nu' - \int_0^\infty (J_{\nu'}+U_{\nu'})\,\Phi_2(\nu,\nu')\,d\nu' \quad (25)$$

were always computed with the mean intensity J_ν on each depth level taken from the initial Thomson scattering model atmosphere, as described in Paper II. This approximation was absolutely necessary to avoid divergence of temperature corrections. However, such a choice certainly introduces some systematic errors.

During a given iteration, tables of both integrals were carefully recomputed for each optical depth τ_d and running frequency ν_i, with new temperatures determined at the end of previous iteration. Therefore Compton scattering contribution to

the equation of transfer was a scalar inhomogeneity changing from one iteration to other, which was just added to the thermal term (Planck function). The same applies to scalars L and L', and all derivatives of Compton scattering functions in the temperature correction term.

Method of solution and elimination scheme were adopted from Madej (1998), and Paper II, with the modifications described above. Convergence of our code was very rapid: in large part the redistribution of external hard X-ray flux to soft X-rays or EUV was computed in the first iteration. Relative temperature correction between neighbouring iterations were very large, and we had to artificially restrict them to max. 3-4, in order to avoid numerical instabilities.

Computer code ATM21 represents implementation and extension of the partial linearization approach, described by Mihalas (1978, pp. 179-180). According to this, we did not linearize neither the variable η, nor dimensionless absorption ϵ.

We have neglected the effects of angular distribution of radiation in Compton scattering integrals just for simplicity. Also we have made other simplification by averaging of nonisotropic Compton scattering differential cross section $\phi(\nu, \nu', \mathbf{n} \cdot \mathbf{n}')$ over cosine of scattering angle, $\mathbf{n} \cdot \mathbf{n}'$. However, it is necessary to point out here that Compton scattering of X-rays can be highly anisotropic, and then the significance of angular effects gets important. Hubeny (2000) expresses opinion, that for photon frequencies $\nu < 10^{19}$ Hz (energies less than 40 keV) the angular effects may easily be more important than errors introduced by the Kompaneets equation approximation (which was rejected in this research).

4. Numerical results

Model atmosphere computations of a B3 V star illuminated by hard X-rays, with temperature T_{rad} almost 4 orders of magnitude higher the T_{eff}, represents a very difficult numerical problem. We have computed two series of Comptonized model atmospheres of the single effective temperature $T_{eff} = 1.8 \times 10^4$ K and gravity $\log g = 4.0$ (cgs units). We have begun our computations adopting models illuminated by isotropic X-rays of diluted thermal spectral distribution with $T_{rad} = 10^8$ K, which were previously computed under assumption of coherent Thomson scattering (Paper II). Isotropy implies, that the true intensity of external irradiation is given by

$$I_\nu^{ext} = w B_\nu(T_{rad}), \tag{26}$$

which defines the dilution factor w.

Model computations with Compton scattering lasted for 16-20 iterations, after which temperature corrections $\Delta T/T$ diminished below 0.005, except for the narrow zone of large temperature drop. In all cases our code reproduces the structure of illuminated models and their spectra for wavelengths ranging from infrared to hard X-rays.

Model atmospheres of the first series assume the presence of hydrogen and helium, with solar number abundance $N_{He}/N_H = 0.11$. In contrast to Paper II, here the hydrogen-helium models can interact with incoming X-ray photons very efficiently via Compton scattering process.

Second series of our models assume hydrogen, helium and iron chemical composition, with number abundances $N_{He}/N_H = 0.11$ and $N_{Fe}/N_H = 3.7 \times 10^{-5}$. In this case iron ions are able to absorb energy of X-ray photons also via thermal absorption.

Similarly as in Paper II, our actual model atmospheres take into account bound-free opacities of 9 lowest levels of hydrogen, 30 levels of neutral helium, and 10 levels of singly ionized helium, supplemented by free-free opacities of their positive ions. The code includes also opacity of hydrogen lines of Lyman, Balmer and Paschen series. The corresponding subroutines were taken from ATLAS 7 code by Kurucz (1985). Iron rich models include rather complex fits to b-f opacities of all existing iron ions (Verner & Yakovlev 1995).

The code includes also very extensive set of LTE bound-free opacities from almost 1000 excited levels of all iron ions, with their threshold energies taken from the Opacity Project database (Seaton 1987). Our computations include also free-free opacities of each iron ion present in the model.

All model atmospheres were computed on very large grid of 1657 wavelength points ranging from 0.03 Å up to 25 000 Å, spaced equidistantly in logarithmic scale. The mesh of standard optical depths consisted of up to 169 points. Standard optical depths were distributed from 10^{-8} on the top of an atmosphere to few times 10^4 at the bottom, depending on the model.

Let us remind here that the outgoing bolometric flux $H_{bol} = 4.736 \times 10^{11}$ cgs roughly equals the external irradiating flux $H_{ext} = 4.512 \times 10^{26}\ w$ at the value of dilution factor $w = 10^{-15}$ (Paper II).

In our computations values of the factor f_ν were either set to 0.33333 as in the Eddington approximation (for the computations of model atmospheres themselves), or iterated precisely as variable Eddington factors (for the final spectrum synthesis).

Iteration of temperature in Comptonized model atmospheres were quite efficient. Particularly in case of H-He models, initial temperatures were always very low, of the order $2 - 3 \times 10^4$ K in a wide range of optical depths above the photosphere. After illuminating that model by hard X-rays, relative temperature corrections initially exceeded one order of magnitude, and we had to diminish them artificially to max. 3-4 in order to ensure stability of temperature iterations. After at least 16 iterations, temperatures in the upper atmosphere could raise to $10^6 - 10^7$ K, which represents a rather dramatic change of physical conditions there. In case of models containing iron, initial temperatures in the uppermost layers were already very high, about 3×10^6 K, and Compton scattering could exert either heating or cooling effect there, depending on the dilution factor w.

As in Paper II, we have averaged temperature corrections over three neighbouring optical depths to prevent temperature fluctuations on the optical depth scale. Moreover, we always computed geometrical average of two temperature distributions corresponding to the last two iterations. This approach enabled us to ensure perfect temperature constancy ($\Delta T/T < 0.0001$) both above the temperature drop and at large depths. Only for the

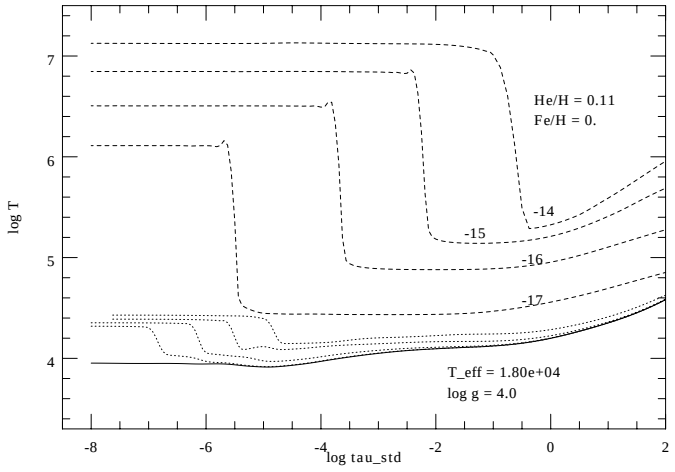

Fig. 1. Run of temperature T vs. standard optical depth, for models with hydrogen and helium. The solid line denotes $T(\tau)$ for nonilluminated atmosphere, whereas dashed lines correspond to atmospheres illuminated by X-rays (Compton scattering). Negative integers attached to dashed lines denote decimal logarithm of the dilution factor w. Dotted lines represent temperatures in illuminated models with Thomson scattering, for the same dilution factors, respectively.

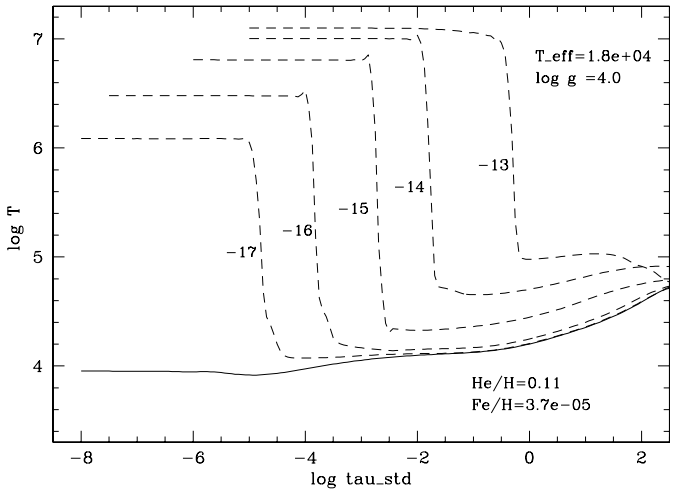

Fig. 2. Run of temperature T vs. standard optical depth, for models with hydrogen, helium, and iron. The solid line denotes $T(\tau)$ for nonilluminated atmosphere, whereas dashed lines correspond to atmospheres illuminated by X-rays, with Compton scattering and various dilution factors.

optical depths surrounding temperature drop, temperature corrections did not reduce satisfactorily even after 16-20 iterations. For all the models we did not exceed 20 iterations, since they were very time consuming. Flux constancy was almost perfect in case of iron reach models, with $\Delta H/H < 2\%$. Unfortunately, in some H-He models flux errors have stabilized on rather high levels exceeding 30%, and further iterations apparently did not tend to lead to better flux constancy.

Flux errors of the above value usually are not acceptable in model atmosphere computations of single stars. In the present research, however, such errors occur in models irradiated by the external X-ray flux of bolometric value 1 - 100 times larger then the own bolometric flux of the atmosphere (equal to 100%). That error value means, that the huge incoming external flux of 100% – 10000% is not perfectly compensated numerically by the same outgoing excess flux. Moreover, we attribute this error also to the fact, that H-He models were computed with too shallow standard optical depth grids, not reaching 10^5.

We have used Pentium II computers, with clock speed of 366 and 600 MHz. A single model atmosphere with Compton scattering has been obtained after 2.5 - 4 days of computations.

4.1. Temperature structure

In all considered models irradiated by the external X-rays, Compton scattering causes very significant effect on temperature run in a stellar atmosphere. In case of pure hydrogen-helium models flux of incoming X-rays heats up atmosphere even by more than three orders of magnitude, as presented in Fig. 1. This is because Compton scattering opacity is the only efficient absorber of X-ray energy, contrary to very small absorption opacity provided by hydrogen and helium ions. Paper II gives an extensive presentation of rather small heating effects, which external X-rays exert in H-He models in presence of coherent Thomson electron scattering (see dotted lines in Fig. 1 of this paper). This is a rather dramatic change of physical conditions in an illuminated atmosphere. In particular, when the irradiating X-ray flux is extremely strong, then the temperature rises by more then 10 times even in the deepest layers, $\tau > 10^5$.

In case of iron rich models, temperatures stabilize also on very high values of the order of millions K (Fig. 2). However, Compton scattering can sometimes diminish temperature of illuminated atmosphere, as compared with models assuming Thomson scattering (Fig. 3). This can occur for weaker external X-ray fluxes, in which case Compton scattering reradiated excess of thermal energy. In previous models with Thomson scattering, iron ions were rather poor emitters of reprocessed energy.

4.2. Outgoing spectra

Fig. 4 presents X-ray and extreme UV spectra for the series of hydrogen-helium models with various dilution factors w. The solid line is the spectrum of LTE nonilluminated model, showing outgoing flux for wavelengths $\lambda > 300$ Å. Dashed lines represent spectra of illuminated models with Compton scattering, whereas dotted lines represent two sample outgoing spectra computed with coherent Thomson scattering (Paper II). One can see dramatic difference between both series of models. Our code with Compton scattering is able to reproduce very significant redistribution effects: practically all the irradiating hard X-ray photons are backscattered as softer photons with energies reduced by few orders of magnitude. Thermal absorption of X-rays by H and He ions is of marginal significance. Flux can increase even by over 15 orders of magnitude due almost solely to Comptonization. Therefore, Compton scattering in our models just creates soft X-ray and extreme UV continuum with

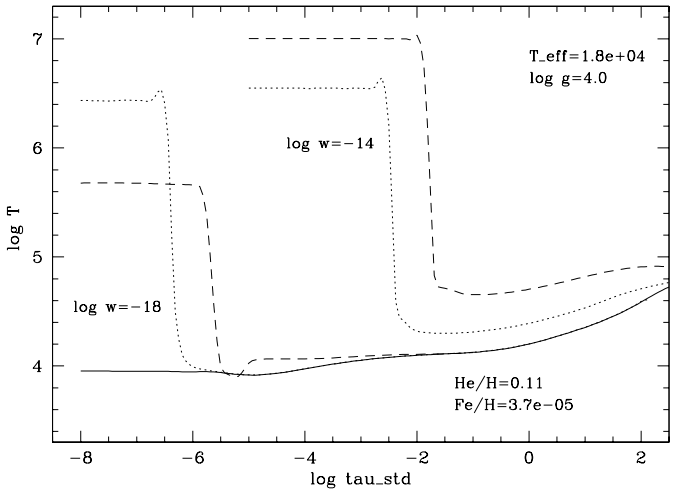

Fig. 3. Comparison between temperature distributions vs. standard optical depth for pairs of models with hydrogen, helium, and iron, for two sample values of the dilution factor w. Dotted lines represent $T(\tau)$ in illuminated atmospheres with coherent Thomson scattering, whereas dashed lines correspond to models with Compton scattering. Note, that Compton scattering can cause either heating or cooling effect, depending on the value of dilution factor (i.e. the value of irradiating X-ray flux).

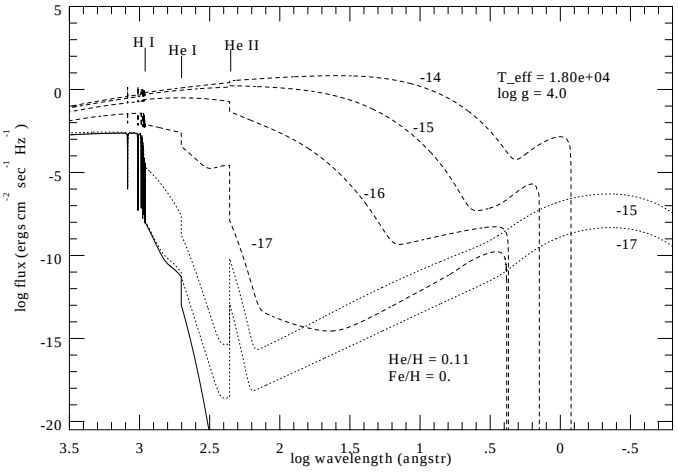

Fig. 4. Spectra of H-He atmospheres in EUV and X-ray wavelengths, for models with Compton scattering (dashed lines), and two sample Thomson scattering models (dotted lines). Compton scattering just creates huge EUV continuum bump, where most of energy is emitted.

distinct hump, which obviously can correspond to soft X-ray excess in AGN. We can also note the existence of distinct Compton cut-off of the outgoing flux.

All spectral features, as hydrogen and helium ionization edges completely disappear due to Comptonization even for low external illumination. This effect can be seen in Fig. 5, which shows series of synthetic spectra around hydrogen Lyman jump at 912 Å. It is obvious, that even for moderate external illumination, $\log w \sim -16$, Lyman jump practically disappears. For stronger external X-ray flux, absorption Lyman lines also disappear and even can reverse to emission.

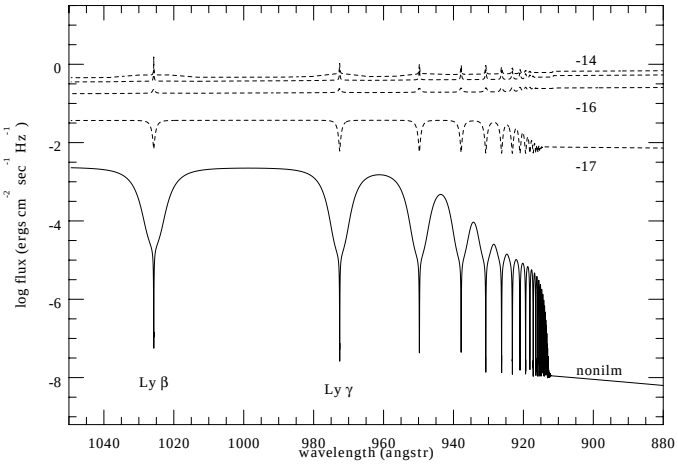

Fig. 5. Set of far UV spectra of Comptonized models at wavelengths around the hydrogen Lyman jump (dashed lines). Solid line represents spectrum of the nonilluminated LTE atmosphere. Lyman b-f jump disappears in all illuminated models due to very strong heating effects. Lyman lines appear in emission for the strongest illumination.

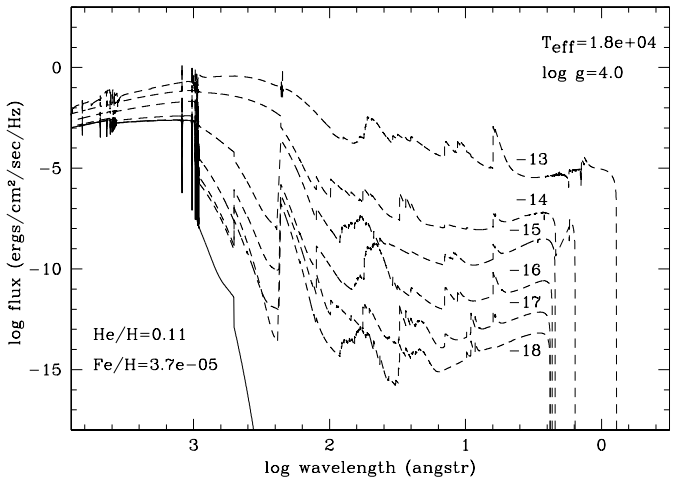

Fig. 6. Spectra of Comptonized iron-rich atmospheres in EUV and X-ray domain. Note huge iron and He II b-f opacity jumps in emission, and Compton cut-off with its energy increasing with increasing dilution factor w.

Fig. 6 presents X-ray and EUV spectra for series of iron rich models. One can easily trace the evolution of spectra with increasing $\log w$. Continuum of those spectra raises very distinctly, however, we did not claim the existence of dominating soft X-ray hump. There exist numerous iron b-f opacity jumps in emission, which can contribute to excess X-ray emission. In all spectra we note the existence of Compton scattering cut-off, with its threshold energy increasing with increasing $\log w$.

Fig. 7 presents two pairs of synthetic X-ray spectra computed either with the account of Compton scattering (dashed lines) or with Thomson scattering (dotted lines). One can easily note that even in iron rich models, Compton scattering raises that part of continuum spectra even by factor 100.

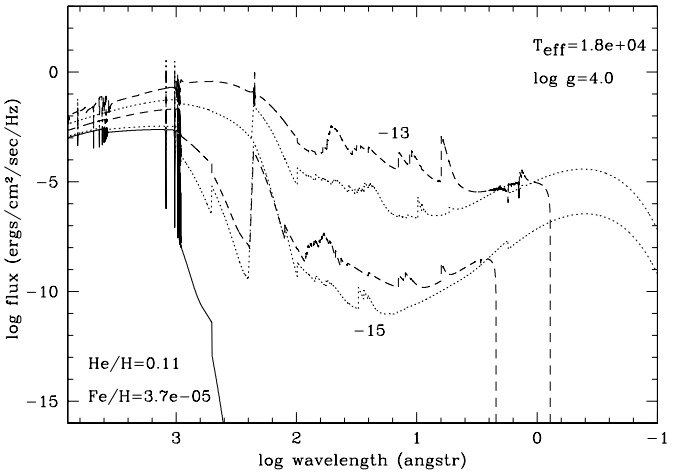

Fig. 7. Comparison between two pairs of iron-rich model spectra, one pair computed with Compton scattering (dashed lines), and remaining pair - with Thomson scattering (dotted lines). Redistribution of hard X-rays by Compton scattering additionally increases EUV and soft X-ray flux by a factor approaching 100.

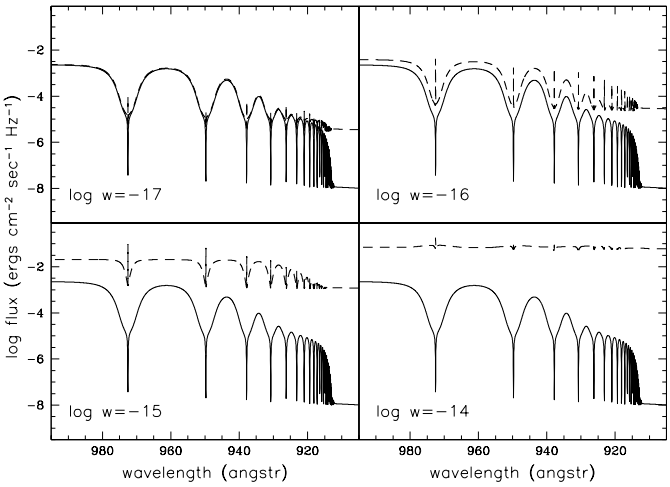

Fig. 8. Evolution of spectra near the hydrogen Lyman jump with increasing external illumination for iron-rich atmospheres (compare to Fig. 5). Again, external X-ray flux efficiently reduces Lyman jump to zero and creates emission cores in numerous Lyman lines.

In case of iron rich models, hydrogen Lyman edge behaves in a slightly different way. Comparison of Fig. 5 and Fig. 8 shows, that significant reduction of the Lyman jump requires much stronger external X-ray flux in iron rich models. At the same time emission cores in Lyman lines are stronger.

We believe, however, that redistribution effects of the incoming X-ray flux are apparently exaggerated, see the outgoing Comptonized spectra in Figs. 4 and 6. Our artificial numerical assumption (Eq. 25) probably causes, that the high energy cut-off exhibited in both figures is too steep. Rejecting of such an assumption probably will result with more soft decrease of the outgoing X-ray flux with increasing photon energy.

5. Discussion

In the previous section we have presented equations of a stellar model atmosphere irradiated by the external hard X-ray flux. In contrast to the existing photoionization codes (cf. Sect. 2), we were able to compute precisely transfer of radiation both in optically thin and thick layers, using all tools of the model stellar atmosphere computations. In other words, our new code ATM21 accurately reproduces radiative transfer and temperature structure both in the hot and cold region simultaneously. At the same time conditions of radiative and hydrostatic equilibrium are rigorously fulfilled. All the models were computed with the LTE equation of state, and with exact treatment of Compton scattering.

As a result, we are able to present and discuss realistic model atmospheres of a B3 V star, isotropically illuminated by very hot X-rays ($T_{rad} = 10^8$ K). We stress here, that the model equations and in particular Compton scattering redistribution formulae are valid for arbitrarily large photon energies and for very hot electrons even with relativistic thermal motion. Also for gas temperatures in which electrons are not relativistic, all the expressions and coefficients in model equations are determined from fully relativistic formulae.

Perhaps the most prominent effect of the external irradiation by X-rays on a stellar atmosphere is the development of high temperature outermost zone, with a very steep temperature drop at some optical depth. This is the penetration depth τ_{pen} defined as

$$\tau_{pen} = \frac{4}{3} w \left(T_{rad}/T_{eff}\right)^4 , \qquad (27)$$

introduced by Hubeny (1990b), who considered analytically the atmosphere of a grey accretion disk with the external illumination. Below the penetration depth the influence of external irradiation gets negligible.

Figs. 1-2 show qualitative agreement with Hubeny (1990b), since our model calculations show that there is distinct temperature jump between the zone with obvious effects of the external illumination, and the deeper zone where heating effects are less pronounced. Both figures demonstrate, that the $\log \tau_{pen}$ increases roughly linearly with $\log w$. There exist, however, very large quantitative differences. For example, at $\log w \sim -15$, Eq. 27 predicts that the penetration depth is of the order unity, whereas model atmospheres plotted in Figs. 1-2 exhibit the transition τ_{pen} two orders smaller. Such a disagreement is not surprising, since the meaning of τ_{std} in our models is different from the meaning of grey optical depth in Hubeny (1990b).

Theoretical spectra of iron-rich models exhibit numerous b-f iron opacity edges in emission, for wavelengths $\lambda < 200$ Å (Fig. 6). They belong to various ionization states, ranging from Fe XVI-XVII (emission edges at 8.48 and 9.15 Å in the spectrum of $\log w = -18$), up to Fe XXIII (edge at 6.25 Å in spectra with larger $\log w$). Hubeny (2000) noted, however, that the identification of Fe ionization states in LTE models is highly inaccurate. He estimates, that in typical NLTE model atmosphere there is a shift of 2-3 iron ionization degrees up, as compared with the LTE model.

In our computations we did not obtain any evidences for thermal instabilities. It is widely believed that such instabilities should develop in illuminated disk atmospheres (Krolik et al. 1981; Różańska & Czerny 1996; Różańska 1999). Most likely we did not encounter such instabilities, because the method of iterating model stellar atmospheres requires the radiative equilibrium, and the numerical methods simply do not allow for ambiguous temperature profile, which can be achieved in simple cooling and heating balance calculations presented by Różańska & Czerny (1996).

This paper was designed for the study of external illumination effects in the atmosphere of a star. However, we believe that the results of our paper can be directly applied to the interpretation of very distinct spectral features observed in AGN. The difference between stellar atmosphere and accretion disk atmosphere is that in the latter case we cannot neglect dissipation of energy via viscous processes. Therefore strict radiative equilibrium cannot be assumed there. Also gravity is not constant across the atmosphere of a disk.

6. Conclusions

We formulated and solved a full set of equations for the LTE model stellar atmosphere in radiative and hydrostatic equilibrium, including both external irradiation and Compton scattering in model equations. Computer code ATM21 used here allowed us to compute precisely radiative transfer and the models with very large relative values of external irradiation fluxes H_{ext} and energies of incident X-ray photons, approaching $m_e c^2$.

We believe, that the model assumptions and numerical results are relevant to accretion disks with hot irradiating coronae in AGN, and their spectral properties.

1. Numerical results presented above clearly demonstrate the nature and the origin of soft X-ray - EUV hump in atmospheres illuminated by external hard X-rays, and in AGN. We prove that the part of spectrum, in which most of the radiative energy is reemitted, is created by redistribution processes in the atmosphere. The redistribution includes either reprocessing by thermal absorption/emission, or Comptonization by electrons colder than the incoming X-rays. The latter process is critically important in stellar/disk atmospheres consisting of hydrogen and helium alone. The importance of thermal emission and absorption increases with increasing abundance of heavy elements (iron).

2. We demonstrate, that the hydrogen Lyman edge exhibits natural tendency to disappear, even for moderate external X-ray fluxes. This occurs in all our models, either with heavy elements (iron) or without them. Disappearance of the Lyman jump occurs in stellar atmospheres with LTE equation of state, and is due to excessive ionization of hydrogen in extremely hot gas. It is not related to possible NLTE effects (Hubeny & Hubeny 1998), but it is solely due to huge temperature rise in the external layers of our illuminated LTE atmospheres.

3. As pointed out by Koratkar & Blaes (1999), practically all spectral lines observed in AGN spectra are seen as emission lines (even without absorption parts). Unfortunately we were unable to compute spectral line profiles, except for hydrogen Lyman and Balmer lines. In most cases of our computations synthetic Lyman and Balmer lines exhibit strong emission cores, sometimes even without any surrounding absorption dips. Since practically all of the LTE b-f opacity jumps appear in emission, we believe that the lacking iron lines will also appear in emission. This is obviously related to very strong temperature inversions in our LTE model atmosphere.

Acknowledgements. We are grateful to Drs. I. Hubeny, A.S. Silbergleit, the referee, and P.T. Życki for their helpful comments and suggestions on the original version of our paper. This research has been supported by grant No. 2 P03D 018 16 from the Polish Committee for Scientific Research.

Appendix: lower boundary condition

At the lower boundary $\tau_{std} = \tau_{max}$ we assume, that the radiation field is thermalized at any considered frequency, $J_\nu(\tau_{max}) = B^*_\nu(\tau_{max})$. Radiation field is isotropic there, and consequently the second moment equals:

$$K_\nu = f_\nu J_\nu = f_\nu \, B^*_\nu \,, \tag{A.1}$$

with the Eddington factors $f_\nu = 0.333333$ at any frequency ν. Asterisk attached to the Planck function indicates, that its value strictly fulfils the condition of radiative equilibrium.

Differentiating Eq. A.1 one can involve the temperature gradient at τ_{max}

$$\frac{\partial}{\partial \tau_\nu}(f_\nu J_\nu) = \frac{1}{3}\frac{\partial B^*_\nu}{\partial \tau_\nu} = \frac{1}{3\eta_\nu(\kappa+\sigma)_{std}\,\rho}\,\frac{\partial B^*_\nu}{\partial T}\,\frac{dT}{dz}\,, \tag{A.2}$$

since $d\tau_\nu = -\eta_\nu(\kappa+\sigma)_{std}\,\rho\,dz$, the ratio $\eta_\nu = (\kappa_\nu+\sigma_\nu)/(\kappa+\sigma)_{std}$, and the dimensionless absorption $\epsilon_\nu = \kappa_\nu/(\kappa_\nu+\sigma_\nu)$.

At the lower boundary we assume also that the diffusion approximation is valid. In this case the bolometric flux is determined by the well known relation

$$H = \frac{1}{3}\int_0^\infty \frac{1}{(\kappa_\nu+\sigma_\nu)\,\rho}\,\frac{\partial B^*_\nu}{\partial T}\,d\nu\,\left(\frac{dT}{dz}\right)\,, \tag{A.3}$$

and is proportional to the gradient of temperature. Bolometric flux $H = \sigma_R T^4_{eff}/4\pi$, where $\sigma_R = 5.66961\times10^{-5}$ (cgs units).

Extracting the gradient dT/dz from the above equation, and substituting to Eq. A.2, we get the lower boundary condition in the form

$$\frac{\partial}{\partial \tau_\nu}(f_\nu J_\nu) \;=\; \frac{H}{\kappa_\nu+\sigma_\nu}\,\frac{\partial B^*_\nu}{\partial T}\,\times \\ \times\left(\int_0^\infty \frac{1}{\kappa_{\nu'}+\sigma_{\nu'}}\frac{\partial B^*_{\nu'}}{\partial T}\,d\nu'\right)^{-1}\,, \tag{A.4}$$

cf. Eq. (7-31) in Mihalas (1978).

Taylor expansion of unknown final values to the first order:

$$T^*(\tau_\nu) = T(\tau_\nu) \,+\, \Delta T(\tau_\nu)\,, \\ B^*_\nu(\tau_\nu) = B_\nu(\tau_\nu) \,+\, \Delta T\,\frac{\partial B_\nu}{\partial T}\,, \tag{A.5}$$

$$\frac{\partial B^*_\nu}{\partial T} = \frac{\partial B_\nu}{\partial T} + \Delta T \frac{\partial^2 B_\nu}{\partial T^2}\,,$$

$$\Phi^*_1(\nu,\nu') = \Phi_1(\nu,\nu') + \left(\frac{\partial \Phi_1}{\partial T}\right)_\tau \Delta T(\tau)\,,$$

$$\Phi^*_2(\nu,\nu') = \Phi_2(\nu,\nu') + \left(\frac{\partial \Phi_2}{\partial T}\right)_\tau \Delta T(\tau)\,.$$

Therefore at a fixed running frequency ν we obtain, after discretization

$$\frac{\partial}{\partial \tau_\nu}(f_\nu J_\nu) = \frac{H}{\kappa_\nu+\sigma_\nu}\left(\frac{\partial B_\nu}{\partial T} + \Delta T \frac{\partial^2 B_\nu}{\partial T^2}\right) \times \times \left[\sum_{i=1}^{I} \frac{w_i}{\kappa_i+\sigma_i}\left(\frac{\partial B_i}{\partial T} + \Delta T \frac{\partial^2 B_i}{\partial T^2}\right)\right]^{-1} \quad \text{(A.6)}$$

Constraint of radiative equilibrium requires that (cf. Eq. 12)

$$\int_0^\infty \eta_\nu \epsilon_\nu \left(J_\nu + U_\nu - B^*_\nu\right) d\nu + + \int_0^\infty \eta_\nu (1-\epsilon_\nu)(J_\nu + U_\nu)\, d\nu \int_0^\infty \Phi^*_1(\nu,\nu')\, d\nu' \quad \text{(A.7)} - \int_0^\infty \eta_\nu (1-\epsilon_\nu)\, d\nu \int_0^\infty (J_{\nu'} + U_{\nu'})\, \Phi^*_2(\nu,\nu')\, d\nu' = 0\,,$$

which yields temperature corrections

$$\Delta T = \frac{\sum_{i=1}^{I} w_i \eta_i \epsilon_i \left(J_i + U_i - B_i\right) + L(\tau)}{\sum_{i=1}^{I} w_i \eta_i \epsilon_i \left(\partial B_i/\partial T\right) - L'(\tau)} = \frac{L_T}{M_T}\,, \quad \text{(A.8)}$$

with U_i denoting the mean intensity of the external illumination.

Let us define auxiliary variables

$$M_1 = \sum_{i=1}^{I} \frac{w_i}{\kappa_i+\sigma_i}\frac{\partial B_i}{\partial T}\,, \quad \text{(A.9)}$$

$$M_2 = \sum_{i=1}^{I} \frac{w_i}{\kappa_i+\sigma_i}\frac{\partial^2 B_i}{\partial T^2}\,, \quad \text{(A.10)}$$

then

$$\frac{\partial}{\partial \tau_\nu}(f_\nu J_\nu) = \frac{H}{\kappa_\nu+\sigma_\nu}\left(\frac{\partial B_\nu}{\partial T} + \Delta T \frac{\partial^2 B_\nu}{\partial T^2}\right) \times \times \left(M_1 + M_2\,\Delta T\right)^{-1} \approx \frac{H\cdot M_1^{-1}}{\kappa_\nu+\sigma_\nu}\frac{\partial B_\nu}{\partial T} \times \times \left[1 + \Delta T \left(\frac{\partial B_\nu}{\partial T}\right)^{-1}\frac{\partial^2 B_\nu}{\partial T^2}\right]\left(1 - \frac{M_2}{M_1}\Delta T\right). \quad \text{(A.11)}$$

Neglecting $(\Delta T)^2$ terms,

$$\frac{\partial}{\partial \tau_\nu}(f_\nu J_\nu) = \frac{H\cdot M_1^{-1}}{\kappa_\nu+\sigma_\nu}\frac{\partial B_\nu}{\partial T} \times \times \left[1 + \Delta T \left(\frac{\partial B_\nu}{\partial T}\right)^{-1}\frac{\partial^2 B_\nu}{\partial T^2} - \frac{M_2}{M_1}\Delta T\right], \quad \text{(A.12)}$$

and, finally

$$\frac{\partial}{\partial \tau_\nu}(f_\nu J_\nu) = \frac{H\cdot M_1^{-1}}{\kappa_\nu+\sigma_\nu}\frac{\partial B_\nu}{\partial T} \times \times \left\{1 + M_T^{-1}\left[\sum_{i=1}^{I} w_i \eta_i \epsilon_i \left(J_i + U_i - B_i\right) + L(\tau)\right] \times \times \left[\left(\frac{\partial B_\nu}{\partial T}\right)^{-1}\frac{\partial^2 B_\nu}{\partial T^2} - \frac{M_2}{M_1}\right]\right\}. \quad \text{(A.13)}$$

The above lower boundary condition can be applied also for the computation of nonilluminated model atmosphere, when we simply set $U_i = 0$ for all $i = 1, \ldots, I$. In case of standard model atmosphere with coherent Thomson scattering, both functions Φ^*_1 and Φ^*_2, and therefore L and L', are also set to zero.

References

Collin-Souffrin S., Czerny B., Dumont A.-M., Życki, P.T., 1996, A&A 314, 393

Guilbert P.W., 1981, MNRAS 197, 451

Hubeny I., 1990a, ApJ 351, 632

Hubeny I., 1990b, Structure and Emission Properties of Accretion Disks. IAU Colloq. 129, 227

Hubeny I., Hubeny V., 1998, ApJ 505, 558

Hubeny I., 2000, private communication

Ko Y.-K., Kallman T.R., 1994, ApJ 431, 273

Koratkar A., Blaes O., 1999, PASP 111, 1

Krolik J.H., McKee C.F., Tarter C.B., 1981, ApJ 249, 422

Kurucz R.L., 1985, private communication

Madej J., 1991, ApJ 376, 161 (Paper I)

Madej J., 1998, A&A 340, 617

Madej J., Różańska A., 2000, A&A 356, 654 (Paper II)

Matt G., Fabian A.C., Ross R.R., 1993, MNRAS 264, 839

Mihalas D., 1978, Stellar Atmospheres. W.H. Freeman and Co., San Francisco

Mushotzky R.F., Done C., Pounds K.A., 1993, A&A 31, 717

Nayakshin S., Kazanas D., Kallman T.R., 2000, in press

Pomraning G.C., 1973, The equations of radiation hydrodynamics. Pergamon Press

Ross R.R., Fabian A.C., 1993, MNRAS 261, 74

Różańska A., 1999, MNRAS 308, 751

Różańska A., Czerny B., 1996, Acta Astron. 46, 233

Ruciński S.M., 1970, Acta Astron. 20, 327

Rybicki G.B., Lightman A.P., 1979, Radiative Processes in Astrophysics. Wiley, New York

Seaton M.J., 1987, J. Phys. B. 20, 6363

Shimura T., Mineshige S., Takahara F., 1995, ApJ 439, 74

Sincell M.W., Krolik J.H., 1997, ApJ 476, 605

Tanaka Y., Lewin W.H.G., 1995, In: Lewin W.H.G., van Paradijs J., van den Heuvel E.P.J. (eds.) Cambridge Astrophys. Ser. Vol. 26, X-ray binaries. Cambridge Univ. Press, Cambridge, p. 126

Turner T.J., Pounds K.A., 1989, MNRAS 240, 833

Verner D.A., Yakovlev D.G., 1995, A&AS 109, 125

Walter R., Fink H.H., 1993 A&A 274, 105

Życki P.T., Krolik J.H., Zdziarski A.A., Kallman T.R., 1994, ApJ 437, 597